

This is the accepted manuscript made available via CHORUS. The article has been published as:

Molecular dynamics study of the adhesion of Cu/SiO₂ interfaces using a variable-charge interatomic potential

Tzu-Ray Shan (山子), Bryce D. Devine, Simon R. Phillpot, and Susan B. Sinnott

Phys. Rev. B **83**, 115327 — Published 24 March 2011

DOI: [10.1103/PhysRevB.83.115327](https://doi.org/10.1103/PhysRevB.83.115327)

Molecular Dynamics Study of the Adhesion of Cu/SiO₂ Interfaces using a Variable Charge Interatomic Potential

Tzu-Ray Shan (單子睿), Bryce D. Devine, Simon R. Phillpot, and Susan B. Sinnott*

Department of Materials Science and Engineering, University of Florida, Gainesville, FL
32611-6400, USA

Abstract

The structural, adhesive, and electronic properties of Cu/ α -cristobalite SiO₂ interfaces with various interface terminations are investigated with molecular dynamics simulations using the charge-optimized many body (COMB) potential. We predict that the Cu/ α -cristobalite interface exhibits the largest adhesion energy for the oxygen-richest condition. The trend of the adhesion energies is consistent with that determined from DFT calculations. We also investigate the properties of Cu/ α -quartz SiO₂ interfaces with different terminations, and show that the trend of adhesion energies is analogous to that of Cu/ α -cristobalite interfaces. The adhesion energies of Cu/amorphous SiO₂ interfaces with different oxygen defect densities are also investigated, and the predicted adhesion energies are compared to experimental values. In particular, it is found that the adhesion energies decrease as the number of oxygen vacancies increases. The calculated charge differences across the interfaces with COMB are also consistent with the DFT electron density difference analysis. These results demonstrate the ability of the empirical, variable charge COMB potential to capture the key physical aspects of heterogeneous interfaces, including predicting that the adhesion of Cu/SiO₂ interfaces increases with interfacial oxygen densities.

*Corresponding author: ssinn@mse.ufl.edu

I. INTRODUCTION

Interfaces between metals and oxides are important because of their ubiquitous presence in numerous materials structures, including microelectronic devices. Copper, one of the most used interconnect material in silicon-based microelectronics and related devices, has low electrical resistivity and high electromigration resistance.^{1,2} It has been reported that high purity Cu films bind well to the silica substrates if there are no hydroxyl groups at the Cu/SiO₂ interface.^{3,4} A major issue, however, is the interaction between Cu and SiO₂ at the interface; this interaction can lead to the formation of oxidized Cu leading to the diffusion of Cu ions through the SiO₂ layer, which results in the degradation of the dielectric layer.^{5,6}

Computational studies of Cu/SiO₂ interfaces using first-principles density functional theory (DFT) calculations have provided valuable insights into the structure and energetics of these interfaces. For example, Nagao et al.⁴ characterized the structural, electronic, and adhesive properties of interfaces between *fcc* Cu (001) and α -cristobalite (001) with different types of interface terminations^{7,8}, and predicted that adhesion at the Cu/SiO₂ interface is the strongest in the most oxygen-rich case. The calculated adhesion energy was consistent with the value obtained experimentally by Kriese et al.⁹ through nanoindentation experiments and Pang et al.¹⁰ through delamination experiments. Although they are effective and provide the highest fidelity currently available, electronic-structure methods are typically limited to systems with a few hundred atoms and are computationally time intensive. As a result of these limitations, such approaches are not easily applied to the study of dynamical processes at finite temperatures.

Atomistic methods, most prominently, molecular dynamics (MD) simulations with empirical interatomic potentials, complement the strengths and weaknesses of electronic-structure methods. The challenge of applying empirical potentials to Cu/SiO₂ interfaces in classical atomistic simulations is the qualitative difference in bonding, metallic versus ionic, between the two constituent components. Furthermore, the simulation must allow for changes in atomic charge as a function of environment, a seemingly inherently

electronic effect. Modeling such interfaces, therefore, has historically been a major challenge to the computational community. The work reported here utilizes classical atomistic simulations with a variable charge interatomic potential to examine the Cu (001)/ α -cristobalite (001) (referred as Cu/ α -C), Cu (001)/ α -quartz (010) (referred as Cu/ α -Q) and Cu (001)/amorphous silica (referred as Cu/a-SiO₂) interfaces. These simulations allow us to extract the structural and adhesive properties, and charge transfer across the interface. The fidelity of the MD simulations is validated against the results of DFT calculations or experimental values for the cases where they are available. The rest of the paper is organized as follows. In Sec. II we introduce methodology utilized in this study, including first-principles calculations and molecular dynamics simulations. In Sec. III, the results for, and the discussion of, the structural and adhesive properties and the charge transfer of the Cu/SiO₂ interfaces is given. Sec. IV contains our conclusions.

II. METHODOLOGY

A. First-principles calculations

To provide reference results against which to compare the results of our atomistic simulations, we perform first-principles density-functional theory calculations of the Cu/ α -C interfaces within the generalized-gradient approximation (GGA),¹¹ using the Perdew–Burke–Ernzerhof (PBE) exchange-correlation functional,¹² as implemented within the Vienna *ab initio* simulation package (VASP).¹³ We use plane-wave basis sets with a 500 eV energy cutoff, and projector augmented-wave (PAW) pseudopotentials^{14, 15} for Si, O, Cu and H. The convergence criteria are set at 1.0×10^{-4} eV and $0.01 \text{ eV} \cdot \text{\AA}^{-1}$ for energies and forces, respectively. We also make use of a Fermi-distribution¹⁶ smearing with a temperature of $k_B T \sim 0.2 \text{ eV}$. For purposes of comparison, we also carry out local density approximation (LDA) calculations with a 394 eV energy cutoff, and used ultrasoft pseudopotentials for Si, Cu and H, and PAW potentials for O. The rest of the computational setups are kept the same as in the GGA calculations. To enable us to make a comparison with the work of Nagao et al.⁴, we examine the same *fcc* Cu (001)/ α -cristobalite (001) interface that they considered in their work.

B. Atomistic simulations with COMB potentials

The variable charge interatomic potentials used for the classical MD simulations are the COMB potentials for Si/SiO₂¹⁷ and Cu/Cu₂O¹⁸, as implemented in the Large-scale Atomic/Molecular Massively Parallel Simulator¹⁹ (LAMMPS) software. These two potentials take the same functional form as described in the COMB potentials for Hf/HfO₂,²⁰ except that additional scaling factors are introduced to the mixing rules for Cu-O and Si-Cu short range interactions. In brief, the COMB formalism takes the general functional form:

$$E_T = \sum_i \left[E_i^S + \frac{1}{2} \sum_{j \neq i} V_{ij}(r_{ij}, q_i, q_j) + E_i^{BB} \right], \quad (1)$$

where E_T is the total potential energy of the system, E_i^S is the self-energy term of atom i , V_{ij} is the interatomic potential between the i th and j th atoms, r_{ij} is the distance between atoms i and j , q_i and q_j are charges of the atoms, and E_i^{BB} is the bond-bending term of atom i . The interatomic potential energy V_{ij} consists of three components: short range repulsion, U_{ij}^R , short range attraction, U_{ij}^A , and long range Coulombic interaction, U_{ij}^I , which are defined as:

$$V_{ij}(r_{ij}, q_i, q_j) = U_{ij}^R(r_{ij}) + U_{ij}^A(r_{ij}, q_i, q_j) + U_{ij}^I(r_{ij}, q_i, q_j) + U_{ij}^V(r_{ij}), \quad (2)$$

$$U_{ij}^R(r_{ij}) = f_{S_{ij}} A_{ij} e^{(-\lambda_{ij} r_{ij})}, \quad (3)$$

$$U_{ij}^A(r_{ij}, q_i, q_j) = -f_{S_{ij}} b_{ij} B_{ij} e^{(-\alpha_{ij} r_{ij})}, \quad (4)$$

$$U_{ij}^I(r_{ij}, q_i, q_j) = J_{ij}(r_{ij}) q_i q_j, \quad (5)$$

$$U_{ij}^V(r_{ij}) = f_{L_{ij}} (C_{VDW_i} C_{VDW_j})^{1/2} / r_{ij}^6. \quad (6)$$

The short range repulsion and attraction leading terms, A_{ij} and B_{ij} , and the inverse decay lengths, λ_{ij} and α_{ij} , are defined as:

$$A_{ij} = \Omega_A \cdot \sqrt{A_{S_i} A_{S_j}}, \quad (7)$$

$$B_{ij} = \Omega_B \cdot \sqrt{B_{S_i} B_{S_j}}, \quad (8)$$

$$\lambda_{ij} = \Omega_\lambda \cdot (\lambda_i + \lambda_j) / 2, \quad (9)$$

$$\alpha_{ij} = \Omega_\alpha \cdot (\alpha_i + \alpha_j) / 2, \quad (10)$$

where Ω_A , Ω_B , Ω_λ and Ω_α are the mixing rule scaling factors.

The many-body effects are described with the bond-order term, b_{ij} , in the short range attraction term, which takes the form

$$b_{ij} = \left[1 + \left(\beta_i \sum_{k \neq i, j} \xi_{ijk} g(\theta_{jik}) \right)^{n_i} \right]^{-1/(2n_i)}, \quad (11)$$

where the symmetry function ξ_{ijk} and angular function $g(\theta_{jik})$ are defined as

$$\xi_{ijk} = f_{S_{ik}} e^{\left[\alpha_{ij}^{m_i} (r_{ij} - r_{ik})^{m_i} \right]}, \quad (12)$$

$$g(\theta_{jik}) = 1 + c_i^2 / d_i^2 - c_i^2 / \left[d_i^2 + (h_i - \cos \theta_{jik})^2 \right]. \quad (13)$$

Here θ_{jik} is the bond angle between bonds ij and ik .

The long-range Coulombic interaction between charged atoms is described with the charge coupling factor, $J_{ij}(r_{ij})$, and takes the form :

$$J_{ij}(r_{ij}) = \int d^3 r_i \int d^3 r_j \rho_i(r_i, q_i) \rho_j(r_j, q_j) / r_{ij}, \quad (14)$$

$$\rho_i(r_i, q_i) = q_i \frac{\xi_i^3}{\pi} e^{(-2\xi_i |r_{ij} - r_i|)}, \quad (15)$$

which is a Coulomb integral over 1s-type Slater orbitals where ξ_i is an orbital exponent that controls the radial decay of the density. A penalty function that captures the change in self energy due to the field of the ionic lattice is added to the self energy term $E_i^S(q_i)$ and takes the form:

$$V_i^S(r, q_j) = \frac{1}{4\pi\epsilon_o} \sum_{j \neq i}^{NN} \left(\frac{\rho_1 q_j^2}{r_{ij}^5} - \frac{\rho_2 q_j}{r_{ij}^5} \right). \quad (16)$$

The self energy term E_i^S describes the energy required to form a charge and takes the form:

$$E_i^S(q_i) = \chi_i q_i + J_i q_i^2 + K_i q_i^3 + L_i q_i^4, \quad (17)$$

where the coefficients χ_i, J_i, K_i , and L_i are fit to the atomic ionization energies and electron affinities.

Bond-bending terms, E_i^{BB} , are applied to Si-O-Si, O-Si-O, Cu-O-Cu, and O-Cu-O bonds, which are defined as:

$$E_{M-O-M} = \sum_i \sum_{j \neq i} \sum_{k \neq i, j} f_{C_{ij}} f_{C_{ik}} K_{M-O-M} (\cos \theta_{M-O-M} - \cos \theta_{M-O-M}^0)^2, \quad (18)$$

$$E_{O-M-O} = \sum_i \sum_{j \neq i} \sum_{k \neq i, j} f_{C_{ij}} f_{C_{ik}} K_{O-M-O} (\cos \theta_{O-M-O} - \cos \theta_{O-M-O}^0)^2, \quad (19)$$

where M is Si or Cu, K_{M-O-M} and K_{O-M-O} are the strengths, and $\cos \theta_{M-O-M}^0$ and $\cos \theta_{O-M-O}^0$ are the ideal bond angles.

The parameterizations for Si, Cu and O are provided in Table I, while the mixing rule scaling factors are provided in Table II. The parameterization of the mixing rule scaling factors is fitted to the adhesion energies of Cu/ α -C interfaces and Cu₂O bulk properties. The Si-Cu mixing scaling factors are only applied to Si-Cu bonds when the Si atom is also bonded to an O atom; the scaling factors are set to 1.0 for all other Si-Cu bonds. However, Cu-O scaling factors are applied to Cu-O bonds regardless of the additional bonding of the Cu atom.

The properties of Cu₂O from the COMB potential compared to experimental and first-principles calculations are given in Table III. It is seen the lattice parameter of Cu₂O from the COMB potential shows ~3% deviation from that from first-principles calculations but the cohesive energy is well reproduced. Some other sets of parameters and mixing rule scaling factors actually give better Cu₂O properties than the set given in Table II; however these scaling factors give worse adhesion energy for Cu/ α -C interfaces. The

properties of Cu and SiO₂ from the COMB potentials can be found in Refs. 21 and 17, respectively.

III. RESULTS AND DISCUSSION

A. Adhesion of Cu/ α -C interfaces

For DFT calculations, the α -cristobalite slab consists of nine SiO₂ layers in the [001] direction with a 2×2 surface unit cell. The dangling O atoms at the bottom are hydrogen-terminated and are fixed at their bulk positions to reduce size effects, while all other atoms are allowed to fully relax. The Cu slab consists of six (001) layers with a 2×2 surface unit cell, whose orientation is rotated 45° about the [001] axis so that the lattice parameter of the 2×2 α -cristobalite slab is well matched to that of the $2\sqrt{2}\times 2\sqrt{2}$ Cu slab. The number of O atoms at the Cu/ α -C interface is varied to mimic oxygen-rich or oxygen-lean conditions, which results in three types of Cu/ α -C interfaces: OO-terminated (Cu/ α -C:OO), O-terminated (Cu/ α -C:O) and Si-terminated (Cu/ α -C:Si) interfaces. The overall thickness of the Cu/ α -C interfacial system is ~ 27 Å. The Monkhorst-Pack k -point mesh²² is $4\times 4\times 1$ for the 9.92 Å $\times 9.92$ Å $\times 45$ Å supercell (with an 18 Å vacuum region). The relaxed structures of the Cu/ α -C:OO, Cu/ α -C:O, and Cu/ α -C:Si interfaces with GGA-PBE viewed along the [100] and [010] directions are shown in Fig. 1 (a) and (b), respectively, which are quite consistent with that obtained with LDA shown in Ref. 4. In particular, the relaxed Cu-O and Cu-Si bond length at the interface from our GGA-PBE calculations are ~ 1.93 Å and ~ 2.47 Å, respectively, compared to ~ 1.90 Å and ~ 2.40 Å, respectively from LDA.⁴ These differences in Cu-O and Cu-Si bond lengths are consistent with the general notion that LDA calculations tend to overestimate bonding energy compared to GGA-PBE calculations.

The Cu/ α -C interfaces for our atomistic simulations using COMB potentials are those used in the DFT calculations, except that the simulation cells have a larger area, and are thicker. Force and energy minimization are applied to find the lowest energy interfacial configurations for the Cu/ α -C:OO, Cu/ α -C:O and Cu/ α -C:Si interfaces, as illustrated in

Figs. 2a and 2b. The minimized Cu/ α -C interfaces from COMB are strikingly similar to those obtained from our GGA-PBE calculations. The minimized Cu-O and Cu-Si bond length at the interfaces from our atomistic simulations are ~ 1.86 Å and ~ 2.32 Å, respectively, which are ~ 5 % smaller than those from GGA-PBE calculations. The smaller Cu-O and Cu-Si bond lengths from COMB potentials compared to DFT calculations come from generally smaller fitted lattice parameters for bulk Cu_2O , as presented in Table III, and SiO_2 phases, as seen in Ref. 17. The adhesion energy, W , is calculated from:

$$W = (E_{\text{SiO}_2} + E_{\text{Cu}} - E_{\text{Cu/SiO}_2}) / A, \quad (20)$$

where E_{SiO_2} , E_{Cu} and $E_{\text{Cu/SiO}_2}$ are the energies of the isolated SiO_2 and Cu slabs and the Cu/ α -C interfaces, respectively, and A is the surface/interface area. The calculated adhesion energies are given in Table IV. The COMB potentials reproduce the same trends for the adhesion energies as the DFT calculations: oxygen-rich interface exhibits the strongest adhesion, followed by intermediate and oxygen-lean interfaces. These are consistent with the notion that Cu films bind well to oxygen-rich SiO_2 substrates. The reason of which is larger numbers of oxidized Cu atoms due to the presence of more O atoms forming Cu-O bonds at the interface. The fidelity of COMB potentials is validated against the results of DFT calculations, and it is proven that COMB potentials are adequate to model Cu/ α -C interfaces. Therefore in the following results and discussion we apply COMB potentials to investigate more Cu/ SiO_2 interfaces.

The intermediate oxygen concentration interface, that is Cu/ α -C:O, considered above is constructed by removing one of the four O atoms from the surface Si from the Cu/ α -C:OO interface. In this case every surface Si is bonded to three O atoms with one O atom bonded to Cu. However, an alternative Cu/ α -C interface with intermediate oxygen concentration can be constructed, which is done by removing two Cu-bonding O atoms from half of the surface Si atoms and remove no oxygen atoms from the other half surface Si atoms. The resulted Cu/ α -C interface is shown in Fig. 3, which can be considered as a hybrid of Cu/ α -C:OO and Cu/ α -C:Si interfaces. The calculated adhesion energy of this hybrid Cu/ α -C interface from COMB potentials is 2.122 J/m^2 , which is slightly smaller than the average adhesion energy of Cu/ α -C:OO and Cu/ α -C:Si interfaces,

which is 2.227 J/m². This smaller than average adhesion energy results from larger Cu-Si distances at the interface, therefore this hybrid Cu/ α -C interface shows weaker Cu-Si interactions than that of the Cu/ α -C:Si interface. Compared to the Cu/ α -C:O interface, on the other hand, this alternative intermediate Cu/ α -C interface has a larger adhesion energy. This is indicative that this intermediate oxygen concentration hybrid interface is more energetically favorable than the original Cu/ α -C:O interface, and that oxygen atoms tend to saturate the bonding between Cu and Si atoms at the Cu/SiO₂ interface, rather than evenly distribute themselves throughout the interface.

B. Adhesion of Cu/ α -Q and Cu/a-SiO₂ interfaces

Since α -quartz is the most stable SiO₂ polymorph and amorphous silica is most widely used in electronic devices, we also investigate the properties of *fcc* Cu (001)/ α -Q (010) and *fcc* Cu (001)/a-SiO₂ interfaces and predict the adhesion energies with the COMB potentials. We create four types of Cu/ α -Q interfaces based on different interface terminations, OO-, O- type I, O- type II, and Si- terminations. The OO-terminated interface has surface O atoms bonded to Si and Cu atoms. Two types of O-terminated interfaces are considered: type I and type II, which are constructed by removing one of the two Wyckoff positions occupied by O atoms. The Si-terminated interface has half surface Si atoms bonded to the Cu slab, the other half Si atoms dangling. Force and energy minimization are applied to find the lowest energy interfacial configurations for the Cu/ α -Q:OO, Cu/ α -Q:O I, Cu/ α -Q:O II and Cu/ α -Q:Si interfaces, as shown in Figs. 4a and 4b. The minimized Cu-O and Cu-Si bond lengths at the interfaces from our MD simulations are ~ 1.91 Å and ~ 2.55 Å, respectively, approximately 3-9% longer than those of the Cu/ α -C interfaces. The predicted adhesion energies are given in Table V. The longer Cu-O and Cu-Si bond lengths are reflective of the slightly smaller adhesion energies for the Cu/ α -Q:OO and Cu/ α -Q:Si interfaces compared to the Cu/ α -C:OO and Cu/ α -C:Si interfaces. However, both type I and type II Cu/ α -Q:O interfaces show $\sim 30\%$ stronger adhesion than the Cu/ α -C:O interfaces. The relatively large difference in adhesion energy for the Cu/ α -Q:O interfaces originated from larger surface energies for the O-terminated α -Q surfaces, averaged 2.6 J/m², compared to that for the O-terminated

α -C surface, 1.3 J/m^2 . Larger surface energies for the O-terminated α -Q surfaces indicate less stable surfaces and also smaller (less negative) numbers for the E_{SiO_2} term used in Eq. 20 to calculate adhesion energies. This is the origin of larger adhesion energies for the Cu/ α -Q:O interfaces. Overall speaking, the trend for the adhesion energies are similar to that of the Cu/ α -C interfaces, and are consistent with the intuition that adhesion energy should increase with the number of oxygen atoms at the interface.

The bulk amorphous silica used in the Cu/a-SiO₂ interfaces are prepared using the melt-and-quench method, as discussed in Ref. 17. The a-SiO₂ slab is created from the bulk a-SiO₂, equilibrated at 300K for 50ps, and then combined with the Cu layer, followed by another 50ps of equilibration at 300K. The equilibrated structure of the Cu/a-SiO₂ interface is illustrated in Fig. 5. Examining the equilibrated interfacial structure, we found the interface Cu atoms are oxidized and acquire charge values from $0.3 \text{ e} \sim 0.6 \text{ e}$. The oxidized Cu atoms and interface O atoms form a thin copper oxide layer with characteristics that resemble the Cu₂O phase. The atomic positions of the second Cu layer are only slightly influenced by the O atoms and the oxidized first Cu layer, and the charge values range from $0.0 \text{ e} \sim 0.1 \text{ e}$. From third Cu layer inward, the Cu atoms retain their bulk *fcc* positions and are charge neutral. This indicates that Cu films oxidize in contact with glass substrates however the oxidation is limited to the first two Cu layers. Examining the bonding between the Cu and a-SiO₂ thin films, the average Cu-O and Cu-Si bond lengths are $\sim 2.04 \text{ \AA}$ and $\sim 2.15 \text{ \AA}$, respectively. We found 22% of the interface Cu atoms are bonded to the glass substrate through Cu-O bonds, and 16% are bonded through Cu-Si bonds; the rest 62% of the interface Cu atoms are not bonded to the a-SiO₂. This bonding statistics reflect the fact that O atoms may play more important roles than Si atoms in terms of bonding the Cu thin film with glass substrates.

To investigate the effect of interfacial defects to the adhesion energy of Cu/a-SiO₂ interface, we introduce oxygen vacancies to the interface and created three Cu/a-SiO₂ interfaces with different numbers of interfacial oxygen defects (V_{O}), 0, 10 and 20, respectively; 10 and 20 oxygen vacancies at the Cu/a-SiO₂ interface correspond to concentrations of 0.565 and $1.130 \text{ } V_{\text{O}}/\text{nm}^2$, respectively. Force and energy are then

minimized with the COMB potentials to calculate the adhesion energies, presented in Table VI, and are compared to the values obtained from experiments.^{10, 23} The predicted adhesion energies of the Cu/ α -SiO₂ interface are reasonably comparable to the experimental values and show the same qualitative trends compared to Cu/ α -C and Cu/ α -Q interfaces: decreasing significantly with the decreased concentration of oxygen atoms at the interface. As presented in Table VI, the percentage of Cu-O bonds at the Cu/ α -SiO₂ interface significantly decreased with the introduction of oxygen vacancies (with 20 vacancies the Cu-O percentage dropped to 11%), while that of the Cu-Si bonds slightly increased. This bonding analysis indicates that Cu-O bonds are the major contributor to the adhesion strength of Cu and SiO₂ substrates. This is due to the strong Coulombic attraction between oxidized Cu atoms and negatively charged O atoms. Additionally, although Cu-Si bonds form at the interface the ionic repulsion strongly reduced their influence to the adhesive strengths.

C. Charge transfer across the Cu/ α -C and Cu/ α -Q interfaces

To examine the charge transfer across the interface and the effect of interface termination to which, we calculate the charge difference, $\delta Q = Q_{Cu/SiO_2} - [Q_{Cu} + Q_{SiO_2}]$, along the interface normal direction; where Q_{Cu/SiO_2} , Q_{Cu} , and Q_{SiO_2} are the distribution of charges of all of the atoms of the Cu/SiO₂ interface system, the individual Cu layer, and the individual SiO₂ slab, respectively. The Cu/SiO₂ interfaces investigated are Cu/ α -C and Cu/ α -Q interfaces. The SiO₂ slab is removed from a fully relaxed, charge equilibrated Cu/SiO₂ interface and a charge equilibration with Cu atoms fixed is carried out to obtain Q_{Cu} . The opposite process is carried out to obtain Q_{SiO_2} . In other words, the physical meaning of the quantity δQ indicates the change in the charge distribution resulting from the chemical bonding between the Cu and α -cristobalite/ α -quartz slabs – an analogous analysis is found in Ref. 4. The charge differences, δQ , for the three original Cu/ α -C interfaces are shown in Fig. 6, while that for the Cu/ α -Q:OO, Cu/ α -Q:O type I, and Cu/ α -Q:Si interfaces are shown in Fig. 7. The charge differences for Cu/ α -C and Cu/ α -Q interfaces show similar behaviors: the difference at the OO-terminated

interface is larger than that at the other two interfaces, indicating the greatest charge transfer at the OO-terminated Cu/SiO₂ interfaces, particularly between Cu and O atoms. The reason for the greatest charge transfer is the largest amount of Cu oxidation due to the increased number of interfacial O atoms. Largest number of Cu-O bonds contributes to the strongest adhesion between the two slabs. The Cu/ α -C result is qualitatively consistent with electron density difference analysis found by DFT.⁴

IV. CONCLUSIONS

To conclude, we have applied empirical, variable charge COMB potentials to examine the Cu/ α -cristobalite, Cu/ α -quartz and Cu/amorphous silica interfaces with different types of terminations that mimic oxygen rich conditions, intermediate and oxygen lean conditions, or different densities of interfacial oxygen defects. We also carried out DFT calculations, both LDA and GGA, to determine the work of adhesion at Cu/ α -cristobalite interfaces; results from these calculations were used to train the COMB potential mixing parameters. The results indicate that the COMB potentials reproduce the structural, adhesive, and electronic properties of the Cu/ α -cristobalite interfaces reasonably consistently with DFT calculations. In addition, the predicted adhesion energies of the Cu/ α -quartz interfaces are consistent with the notion that adhesion is the strongest for oxygen rich conditions. The COMB potential was further applied to predict the adhesion energies of Cu/a-SiO₂ interfaces with different concentrations of interfacial oxygen vacancies. The results indicate that the adhesion energy decreases as the number of oxygen vacancies increases due to decreased Cu-O bonds. The COMB potential for Si/SiO₂/Cu/Cu₂O is shown to be adequate for carrying out variable charge MD simulations of Cu/SiO₂ interfaces, and this should pave the way for significant progress in modeling these types of challenging interfaces.

ACKNOWLEDGMENTS

We gratefully acknowledge the financial support of the National Science Foundation under grant number DMR-0426870 and a grant of computer time from the High Performance Computing Center at the University of Florida.

REFERENCES

- ¹ S. P. Murarka, Mater. Sci. Eng., R **19**, 87 (1997).
- ² M. Hasan, and J. F. Rohan, J. Electrochem. Soc. **157**, D278 (2010).
- ³ S. P. Murarka, R. J. Gutmann, A. E. Kaloyeros, and W. A. Lanford, Thin Solid Films **236**, 257 (1993).
- ⁴ K. Nagao, J. B. Neaton, and N. W. Ashcroft, Phys. Rev. B **68**, 125403 (2003).
- ⁵ J. Cechal, J. Polcak, M. Kolibal, P. Babor, and T. Sikola, Appl. Surf. Sci. **256**, 3636.
- ⁶ Y. L. Cheng, T. J. Chiu, B. J. Wei, H. J. Wang, J. Wu, and Y. L. Wang, J. Vac. Sci. Technol., B **28**, 567 (2010).
- ⁷ P. Hohenberg, and W. Kohn, Phys. Rev. B **136**, B864 (1964).
- ⁸ W. Kohn, and L. J. Sham, Phys. Rev. **140**, 1133 (1965).
- ⁹ M. D. Kriesse, N. R. Moody, and W. W. Gerberich, Acta Mater. **46**, 6623 (1998).
- ¹⁰ M. Z. Pang, and S. P. Baker, J. Mater. Res. **20**, 2420 (2005).
- ¹¹ J. P. Perdew, J. A. Chevary, S. H. Vosko, K. A. Jackson, M. R. Pederson, D. J. Singh, and C. Fiolhais, Phys. Rev. B **46**, 6671 (1992).
- ¹² J. P. Perdew, K. Burke, and M. Ernzerhof, Phys. Rev. Lett. **77**, 3865 (1996).
- ¹³ G. Kresse, and J. Furthmüller, Phys. Rev. B **54**, 11169 (1996).
- ¹⁴ G. Kresse, and D. Joubert, Phys. Rev. B **59**, 1758 (1999).
- ¹⁵ P. E. Blochl, Phys. Rev. B **50**, 17953 (1994).
- ¹⁶ M. Methfessel, and A. T. Paxton, Phys. Rev. B **40**, 3616 (1989).
- ¹⁷ T.-R. Shan, B. D. Devine, J. W. Hawkins, A. A. Asthagiri, S. R. Phillpot, and S. B. Sinnott, Phys. Rev. B **82**, 235302 (2010).
- ¹⁸ B. D. Devine, T.-R. Shan, M.-Y. Lee, A. McGaughey, S. B. Sinnott, and S. R. Phillpot, (unpublished).
- ¹⁹ S. J. Plimpton, J. Comput. Phys. **117**, 1 (1995).

- ²⁰ T. R. Shan, B. D. Devine, T. W. Kemper, S. B. Sinnott, and S. R. Phillpot, Phys. Rev. B **81**, 125328 (2010).
- ²¹ J. Yu, S. B. Sinnott, and S. R. Phillpot, Philos. Mag. Lett. **89**, 136 (2009).
- ²² H. J. Monkhorst, and J. D. Pack, Phys. Rev. B **13**, 5188 (1976).
- ²³ T. S. Oh, R. M. Cannon, and R. O. Ritchie, J. Am. Ceram. Soc. **70**, C352 (1987).
- ²⁴ J. Hallberg, and R. C. Hanson, Physica Status Solidi **42**, 305 (1970).

Tables

Table I: Parameterizations of Si, O and Cu for the COMB potentials

	Si	O	Cu
A (eV)	1803.81	3326.70	952.693
B (eV)	471.17	260.89	146.987
λ (\AA^{-1})	2.4799	5.36	2.794608
α (\AA^{-1})	1.7322	2.68	1.681711
β	1.0999×10^{-6}	2.0	0.140835
n	0.78734	1	1
m	3	1	1
c	100390	6.6	0
d	16.218	1	1
h	-0.59826	-0.229	0
R_S (\AA)	2.6	2.6	2.85
S_S (\AA)	3.0	3.0	2.95
Q_L	-4.0	-1.8349	-6.0
Q_U	4.0	5.5046	2.0
D_L	1.651725	0.00148	0.16776
D_U	-1.658949	-0.00112	-0.16100
X(eV)	0	5.6344	0
J(eV)	3.6251	7.6896	5.946437
K(eV)	0	4.5143	0
L(eV)	0.0870	1.3301	0

ξ	0.7729	2.2431	0.454784
ρ_1	-0.4994	-3.9220	0.72571
ρ_2	2.9999	0.9711	0.274649
K_{M-O-M} (eV)	2.60	--	0.007858
K_{O-M-O} (eV)	0.3122	--	2.518789
$\cos\theta^0_{M-O-M}$	143.73	--	109.47
$\cos\theta^0_{O-M-O}$	109.47	--	180.0
C_{VDW}	0.0	0.0	0.0

Table II: Mixing rule scaling factors for Si-O, Si-Cu and Cu-O pairs.

	Si-O	Si-Cu	Cu-O
Ω_A	1.0	1.276957	1.666072
Ω_B	1.0	0.452693	0.100000
Ω_λ	1.0	1.032042	1.097775
Ω_α	1.0	1.354486	0.584713

Table III: Properties of Cu₂O calculated with the COMB potentials compared to that from experiments and DFT calculations.

Properties	Expt. ²⁴	DFT-PBE	COMB
a ₀ (Å)	4.274	4.267	4.226
E _c (eV/Cu ₂ O)		-11.34	-11.91
C ₁₁ (GPa)	123	126	105
C ₁₂ (GPa)	107	106	89
C ₄₄ (GPa)	12	15	71
B (Gpa)	112	113	94
G (Gpa)	8	10	45
q _{Cu} (e)		0.55	0.79

Table IV: Adhesion energies (in units of J/m²) of the *fcc* Cu (001)/ α -cristobalite (001) interfaces from Ref. ⁴ (first DFT-LDA column), our DFT calculations (second DFT-LDA column and DFT-GGA column), and MD simulations using COMB potentials (COMB column). Cu/ α -C:OO, Cu/ α -C:O and Cu/ α -C:Si denotes OO-, O- and Si- terminated Cu/ α -C interfaces, respectively.

Type of interface	W (J/m ²)			
	DFT-LDA ⁴	DFT-LDA	DFT-GGA	COMB
Cu/ α -C:Si	1.406	1.432	1.034	0.864
Cu/ α -C:O	1.555	1.591	1.222	1.734
Cu/ α -C:OO	3.805	3.987	3.601	3.591

Table V: Adhesion energies (in units of J/m^2) of the *fcc* Cu (001)/ α -quartz (010) interfaces from MD simulations using COMB potentials. Cu/ α -Q:Si, Cu/ α -Q:O I, Cu/ α -Q:O II and Cu/ α -Q:OO denotes Si-, O- type I, O- type II and OO- terminated Cu/ α -Q interfaces, respectively.

Type of interface	W (J/m^2)
Cu/ α -Q:Si	0.850
Cu/ α -Q:O I	2.494
Cu/ α -Q:O II	2.646
Cu/ α -Q:OO	3.472

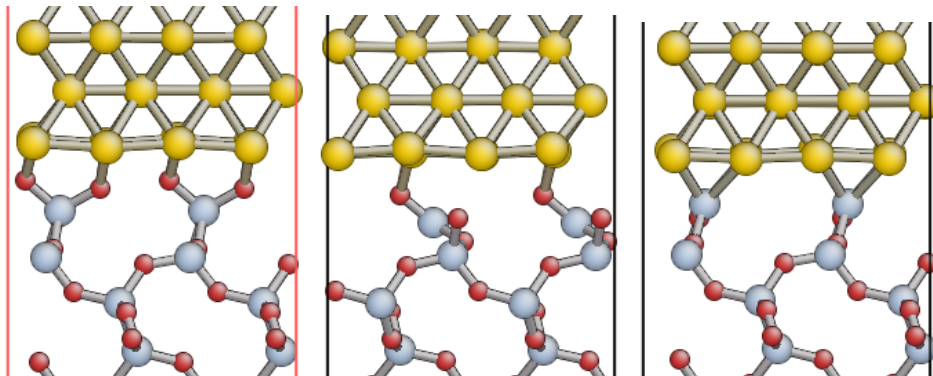
Table VI: Adhesion energies (in units of J/m²) of the Cu/a-SiO₂ interfaces with different numbers of oxygen vacancy defects from MD simulations using COMB potentials. Experimental adhesion energy values from the literature for Cu/a-SiO₂ interface and the bonding analysis between Cu and a-SiO₂ are also given.

Type of interface	W (J/m ²)		Interfacial Cu bonding (%)		
	Exp	COMB	Cu-O	Cu-Si	Non-bonded Cu
Cu/a-SiO ₂ + 0 V _O	0.5 - 1.2 ²³ 0.6 - 1.4 ¹⁰	1.810	22	16	62
Cu/a-SiO ₂ + 10 V _O		0.629	13	18	79
Cu/a-SiO ₂ + 20 V _O		0.289	11	19	80

Figures

Figure 1: (Color online) Relaxed structures of the *fcc* Cu (001)/ α -cristobalite (001) interfaces, OO-, O-, and Si-terminated, respectively, with DFT-PBE calculations viewing along (a) [100] and (b) [010] directions. Cu layer on the top, SiO₂ layer on the bottom (larger spheres are Si, smaller ones are O).

(a)



(b)

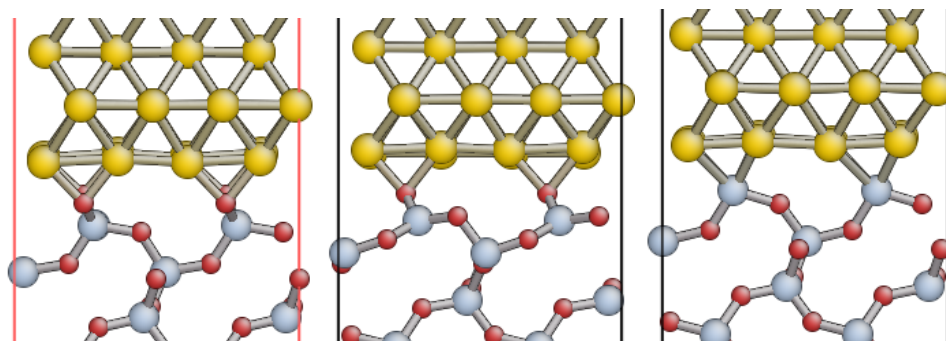
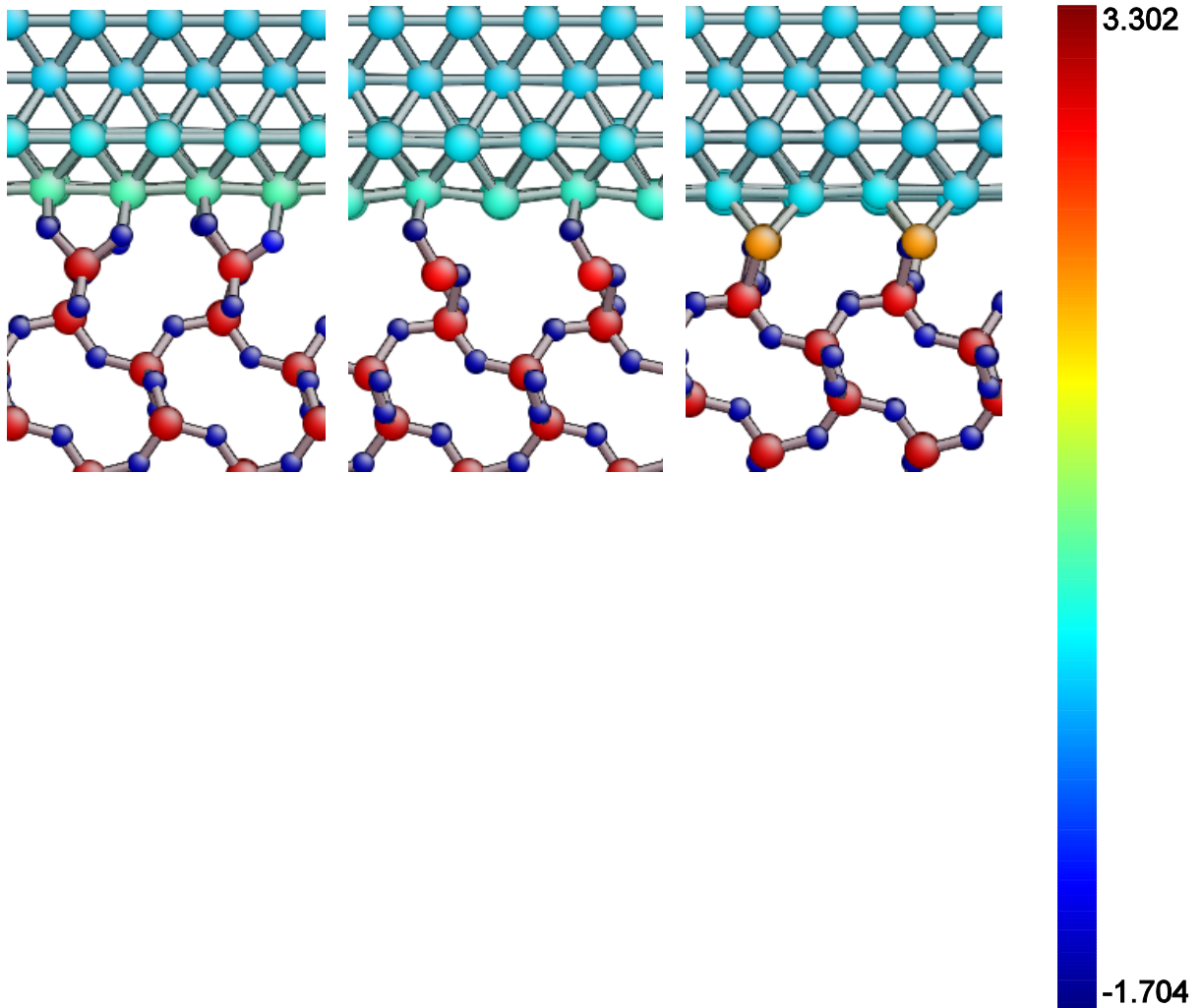


Figure 2: (Color online) Minimized structures of the *fcc* Cu (001)/ α -cristobalite (001) interfaces, OO-, O-, and Si-terminated, respectively, with MD simulations using the COMB potentials viewing along (a) [100] and (b) [010] directions. Cu layer on the top, SiO₂ layer on the bottom. Atoms are color coded by the charge values indicated by the color bar (navy is negatively charged, cyan is charge-neutral, and red is positively charged).

(a)



(b)

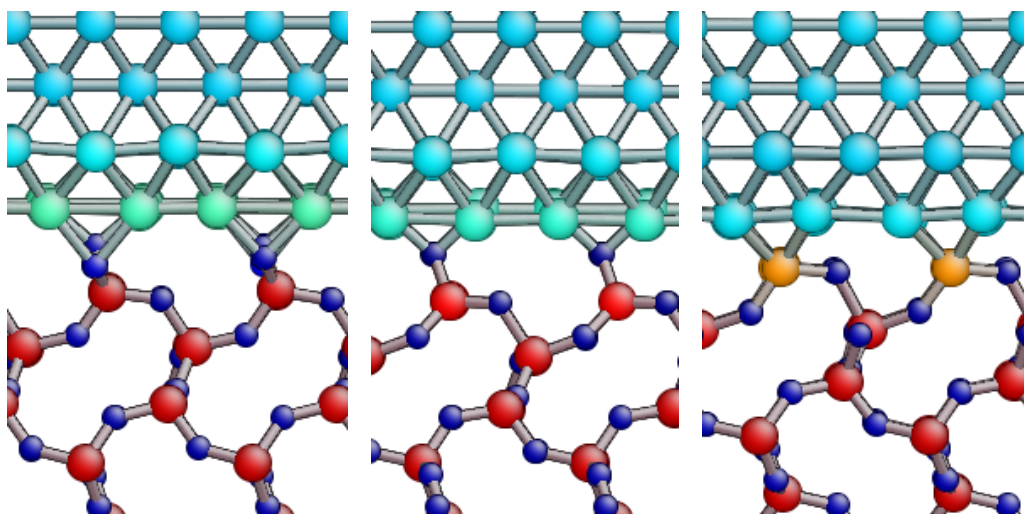
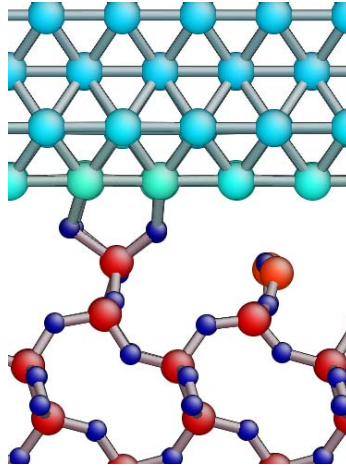


Figure 3: (Color online) Minimized structures of an alternative intermediate oxygen concentration *fcc* Cu (001)/ α -cristobalite (001) interface with MD simulations using the COMB potentials viewing along (a) [100] and (b) [010] directions. Color code is the same as that of Fig. 2.

(a)



(b)

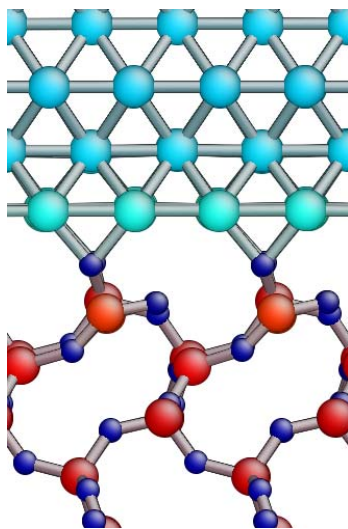
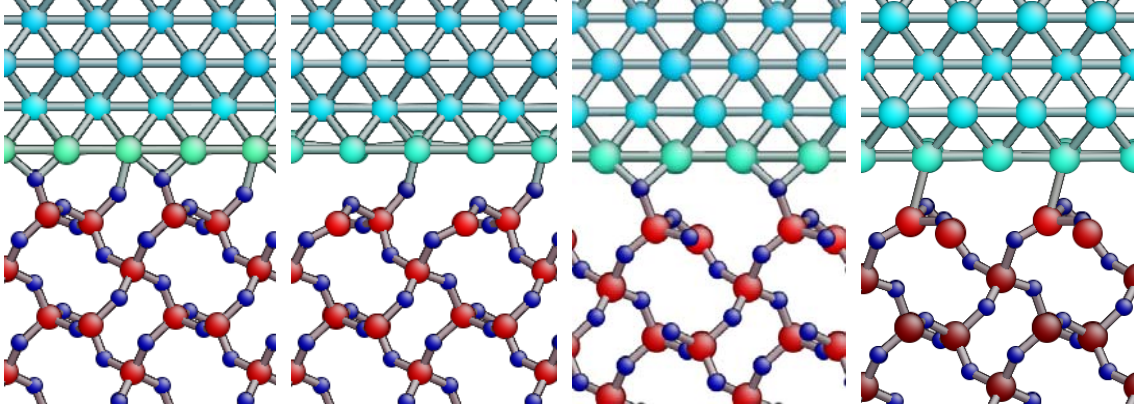


Figure 4: (Color online) Minimized structures of the *fcc* Cu (001)/ α -quartz (010) interfaces, OO-, O- type I, O- type II, and Si-terminated, respectively, with MD simulations using the COMB potentials viewing along (a) [100] and (b) [001] directions. Color code is the same as that of Fig. 2.

(a)



(b)

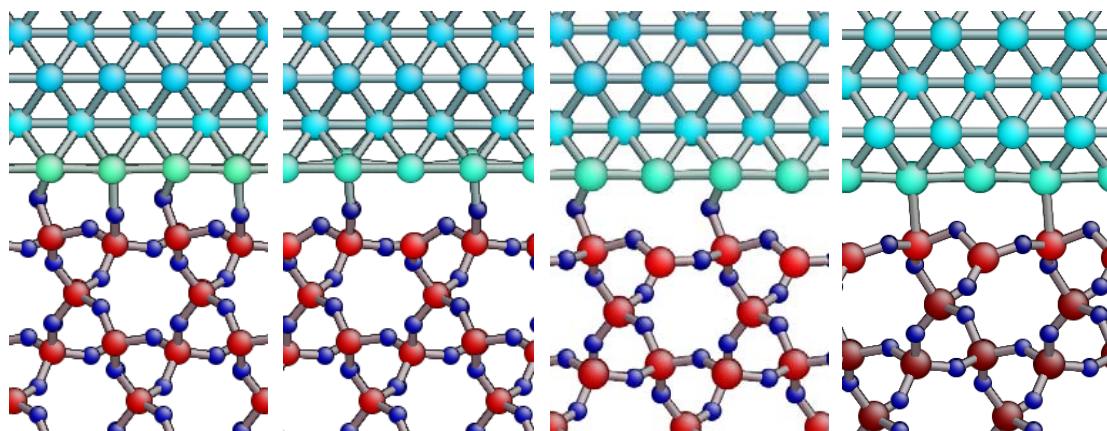


Figure 5. (Color online) Minimized structures of the fcc Cu (001)/a-SiO₂ + 0 VO interfaces with MD simulations using the COMB potentials. Color code is the same as that of Fig. 2.

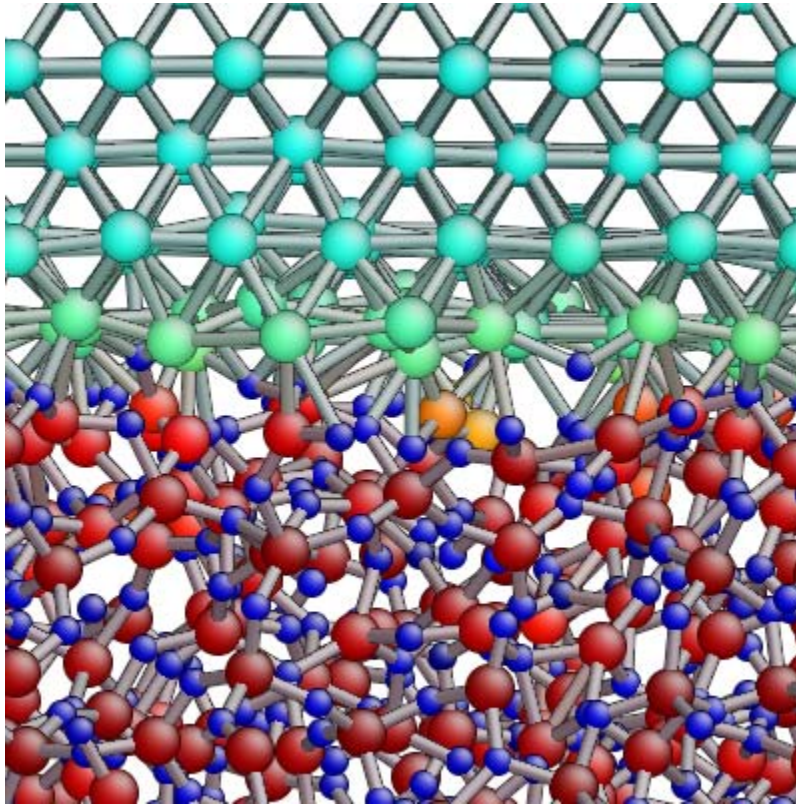


Figure 6: (Color online) Charge difference across the *fcc* Cu (001)/ α -cristobalite (001) interfaces. The Cu slab is to the right of the interface; the SiO₂ slab is to the left of the interface.

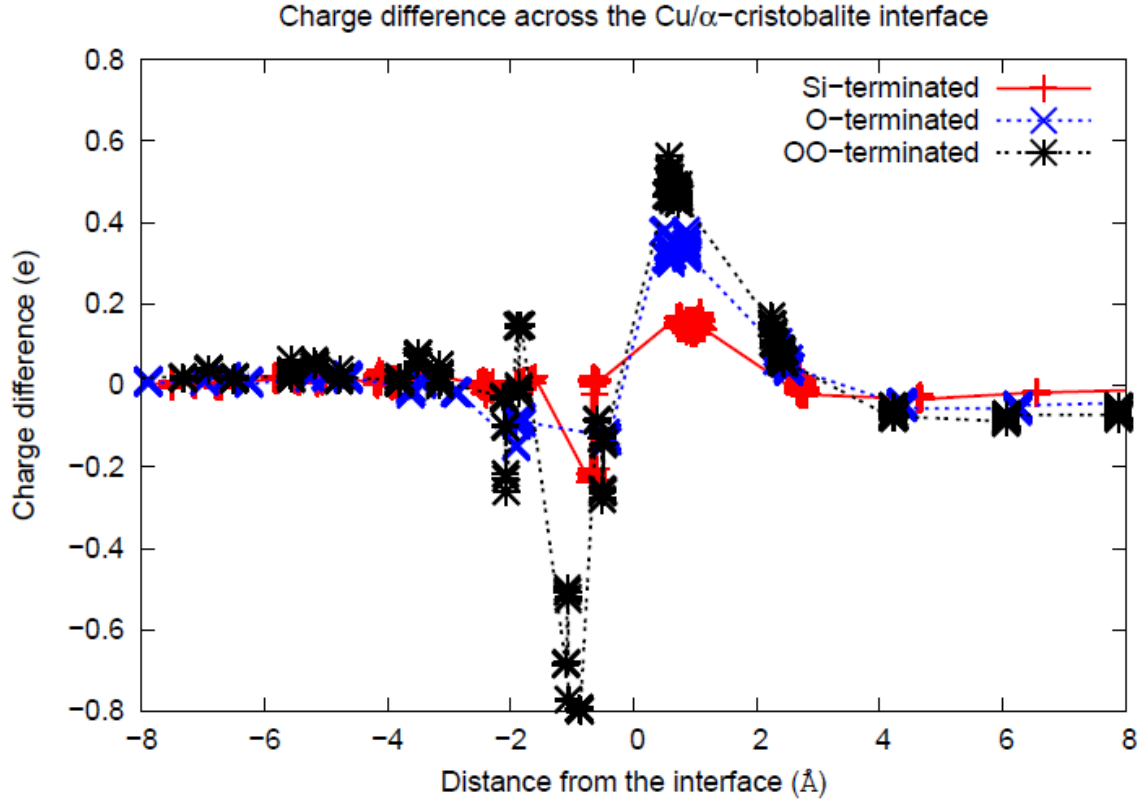


Figure 7: (Color online) Charge difference across the *fcc* Cu (001)/ α -quartz (010) interfaces. The Cu slab is to the right of the interface; the SiO₂ slab is to the left of the interface.

